Achieving 21% External Quantum Efficiency for Non-doped Solution-Processed Sky-Blue Thermally Activated Delayed Fluorescence OLEDs by Means of Multi-Donor/Acceptor Emitter with Through-Space/-Bond Charge Transfer

Xujun Zheng, Rongjuan Huang, Cheng Zhong, Guohua Xie, Weimin Ning, Manli Huang, Fan Ni, Fernando B. Dias,* and Chuluo Yang**

Dr. X. Zheng, Dr. C. Zhong, W. Ning, M. Huang, Prof. G. Xie, Prof. C. Yang,
Renmin Hospital of Wuhan University, Hubei Key Lab on Organic and Polymeric Optoelectronic Materials, Department of Chemistry, Wuhan University, Wuhan 430072, P. R. China.
E-mail: clyang@whu.edu.cn, guohua.xie@whu.edu.cn

Dr. X. Zheng, Dr. F. Ni, Prof. C. Yang,
Shenzhen Key Laboratory of Polymer Science and Technology, College of Materials Science and Engineering, Shenzhen University, Shenzhen 518060, China.
E-mail: clyang@szu.edu.cn

Dr. R. Huang, Prof. F. B. Dias,
Department of Physics, Organic Electroactive Materials Group, Durham University, Durham, United Kingdom.
E-mail: f.m.b.dias@durham.ac.uk

Abstract

Although numerous thermally activated delayed fluorescence (TADF) organic light-emitting diodes (OLEDs) have been demonstrated, the efficient blue or even sky-blue TADF-based non-doped solution-processed devices are still very rare. Herein, we skilfully incorporate through-space charge transfer (TSCT) and through-bond charge transfer (TBCT) effect, as well as the multi-(donor/acceptor) characteristic into one molecule. The former allows this material to show small singlet-triplet energy splitting (ΔE_{ST}) and high transition dipole moment. The latter, on one hand, further lights up multi-channel reverse intersystem crossing (RISC) to increase triplet exciton utilization *via* degenerating molecular orbitals. On the other hand, the nature of the molecular twisted structure effectively suppresses intermolecular packing to obtain high PLQY in neat flims. Consequently, using this design strategy, **T-CNDF-T-*t*Cz** containing three donor and three acceptor units, successfully realizes an extremely small ΔE_{ST} (~ 0.03 eV) and a high PLQY (~ 0.76) at the same time, hence the non-doped solution-processed sky-blue TADF-OLED displays record-breaking efficiency among the solution processes-based non-doped sky-blue OLEDs, with high brightness over 5200 cd m^{-2}, current efficiency up to 46.4 cd A^{-1}, and external quantum efficiency up to 21.0%.

keywords: non-doped solution-processed OLED, sky-blue, thermally activated delayed fluorescence, through-space/-bond charge transfer, multi-(donor/acceptor)

Owing to their superior display quality and flexibility, organic light-emitting diodes (OLEDs) have been leading the innovation in flat panel displays and lighting applications. Unfortunately, the spin statistics makes OLEDs using conventional organic fluorescent emitters very inefficient, with an upper limit to their internal quantum efficiency (IQE) of 25% due to the fact that only one-quarter of the excitons are singlets.[1] However, thermally activated delayed fluorescence (TADF) emitters, pioneered by C. Adachi, can utilize the up-conversion from triplet to singlet states through reverse intersystem crossing (RISC). Thus, nearly 100% IQE could be obtained in noble-metal-free electroluminescence (EL) device.[2-6] Moreover, TADF materials would help to overcome the putative disadvantages of Ir or Pt-containing systems,[7-9] such as the relatively high cost and scarce resources, and potential environmental problems.

To date numerous highly efficient TADF-based OLEDs have been successfully reported,[10-19] including solution-processed blue emitting devices.[20, 21] Since this manufacturing technique is amenable to the industrialization of OLEDs, due to its natural distinctive advantages, such as the low-cost, high processing efficiency, easy scalability, and better controlling of the doping concentration.[22, 23]

In 2018, Kaji *et al.* applied an adamantyl substitution strategy to access solution processable blue TADF-OLEDs with external quantum efficiency (EQE) of up to 22%.[24] However, these devices required the TADF material being used as a dopant in different hosts, which makes its manufacturing process too complicated, as well as rendering poor repeatability and stablility. Therefore, this strategy is not favorable for large-scale industrial production. Earlier, in 2017,

the Lu's group reported a non-doped solution-processed blue TADF-OLED, but the efficiency was less than 20%.[25] Highly efficient OLEDs, with blue or even sky-blue emission, based on TADF non-doped layers, and fabricated by solution-processed methods are still very rare, and remain a great challenge.

Herein, we report a charge-transfer-featured TADF emitter, namely **T-CNDF-T-*t*Cz** (vide **Figure 1a**), with three alternative donor and three acceptor units, in which di-*tert*-butylcarbazole (***t*Cz**), benzene (**ph**) and difluorocyanobenzene (**CNDF**) act as an electron donor, a π-bridge, and an electron acceptor, respectively. Due to the fact that the D and A units in **T-CNDF-T-*t*Cz** are connected to the central benzene bridge by alternating arrangement, the spatial vertical distance between D and A was decreased while the twisted angles of D (or A) with benzene group were increased. As expected, on one hand, the alternating arrangement of D-A units endows **T-CNDF-T-*t*Cz** the coexistence of through-space charge transfer (TSCT) and through-bond charge transfer (TBCT) effects, resulting in a small ΔE_{ST} and high PLQY.[26] On the other hand, the multi-(donor/acceptor) structure in **T-CNDF-T-*t*Cz** promotes spin-vibronic mixing among the multiple excited states, which is crucial to the efficient multi-channel RISC process.[10] Remarkably, its highly twisted structure could suppress the intermolecular π-π stacking, leading to reduced fluorescence quenching in condensed state.[27, 28] Therefore, the non-doped solution-processed sky-blue TADF-OLED displays high performance with a brightness (B_{max}) over 5200 cd m^{-2}, and maximum external quantum efficiency (EQE_{max}) up to 21.0%, which represents the record-breaking EL efficiency among the solution process-based non-doped blue or sky-blue

devices. In contrast, the reference molecules with fewer donor/acceptor fragments, **S-CNDF-S-*t*Cz** and **S-CNDF-D-*t*Cz** (see **Figure 1a**), show less efficient RISC processes and lower PLQYs. Consequently, the corresponding devices render inferior performances. Our results indicated that such multi-(donor/acceptor) TADF molecules combined with TSCT and TBCT effects should be promising TADF emitters, and may shed light on the molecular design to achieve high-performance OLEDs.

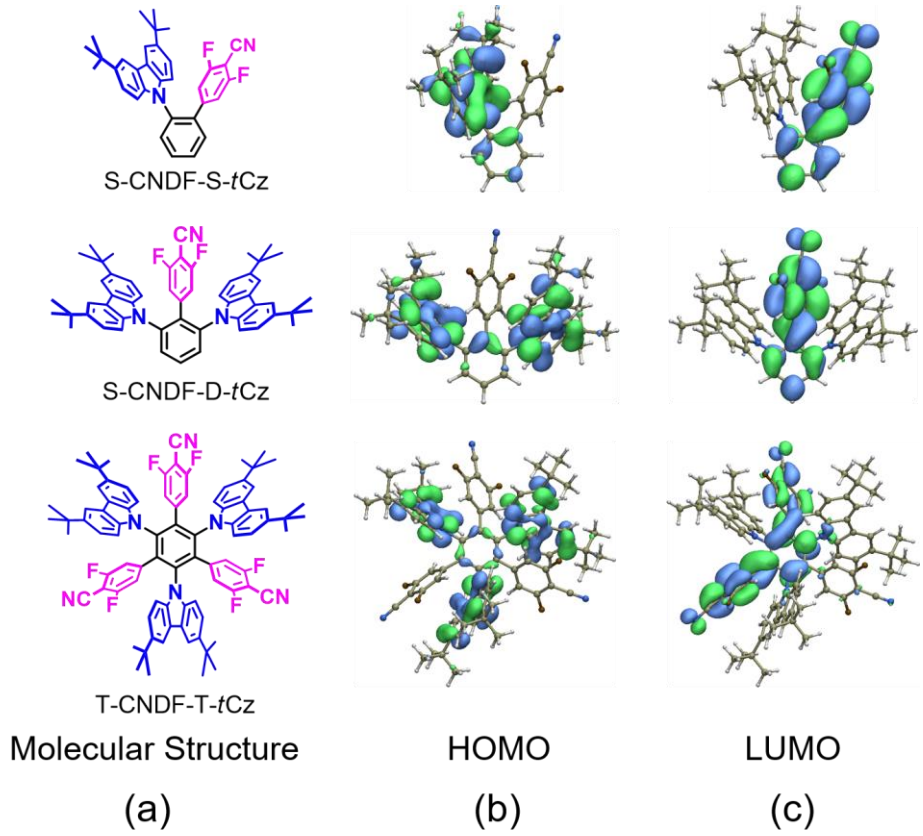

Figure 1. The molecular structures (a), HOMO (b) and LUMO (c) distributions of **S-CNDF-S-*t*Cz** (top), **S-CNDF-D-*t*Cz** (middle), and **T-CNDF-T-*t*Cz** (bottom).

According to our design strategy, the donor group *t*Cz and the acceptor CNDF group are connected on the benzene ring by mutual *ortho*-position, which generates an interchromophore packing with a distance less than 3.3 Å, the effective van der Waals

distance. Hence, charge could be transferred through space and linker simultaneously in **T-CNDF-T-*t*Cz**, achieving a balance between small ΔE_{ST} and high PLQY (Φ_{PL}). Moreover, the multi-(donor/acceptor) architecture could further enhance PLQY with the intermolecular stacking inhibited, and accelerate the RISC process due to the degenerated excited state. The design strategy was guided by time-dependent density functional theory (TD-DFT) based on the PBE0 functional and a def2-SVP basis. As shown in **Figure 1Sb**, in the optimized structure of **T-CNDF-T-*t*Cz**, the dihedral angles of *t*Cz and CNDF with the linker ph are 73.7^{o} and 56.2^{o}, respectively, and the minimum spatial distance between D and A is less than 3.3 Å, suggesting a more effective intramolecular π-π interaction between donor and acceptor, *i.e.*, TSCT, compared with the reference compounds (50.8^{o} and 47.8^{o} for **S-CNDF-S-*t*Cz**, and 57.0^{o} and 55.7^{o} for **S-CNDF-D-*t*Cz**, respectively).

In view of the frontier molecular orbital (FMO), the highest occupied molecular orbital (HOMOs) of these molecules are mainly located on the *t*Cz units (**Figure 1b**), while the lowest unoccupied molecular orbital (LUMOs) distribute in the CNDF units (**Figure 1c**). The spatial separated HOMO and LUMO may ensure that the emitters own the small ΔE_{ST}s to guarantee a valid TADF. It is worth mentioning that the phenyl bridges are all involved in contributing their frontier orbitals, which suggests that charge can also be transferred through the linker directly, *i.e.*, TBCT. The proportions of TBCT/TSCT can be obtained by integrating the transition density that is localized on/not on the benzene bridge. According to the calculations, the proportions of TSCT/TBCT in S1 state of **T-CNDF-T-*t*Cz**, **S-CNDF-D-*t*Cz**, and **S-CNDF-S-*t*Cz** are 77.2%/22.8%, 76.5%/23.5%, and 63.7%/36.3%, respectively.

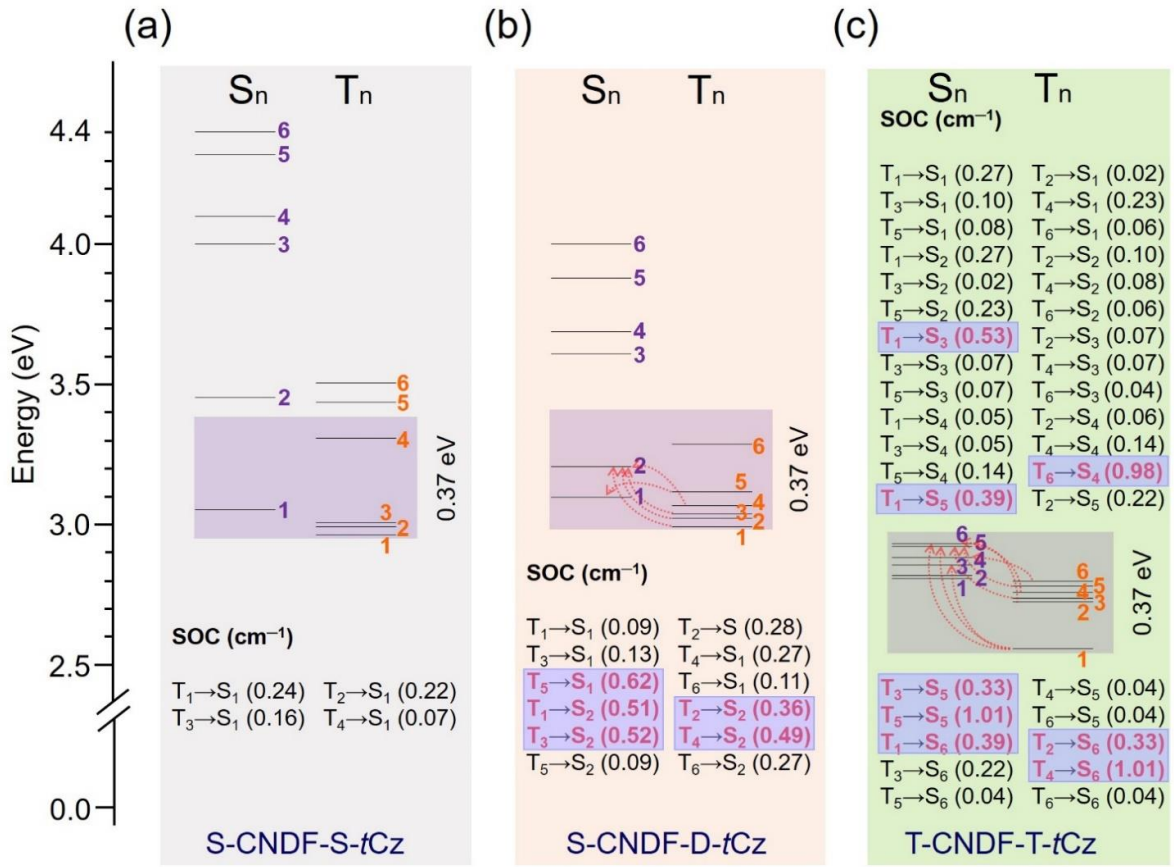

Figure 2. Proposed mechanism for facile RISC channel (both $\Delta E_{ST} \leq 0.37$ eV, and SOC ≥ 0.3 cm^{-1})[29, 30] in multi-(donor/acceptor)-based TADF materials. TD-DFT calculated energy level diagram and the corresponding SOC constants of **S-CNDF-S-*t*Cz** (a), **S-CNDF-D-*t*Cz** (b), and **T-CNDF-T-*t*Cz** (c). The valid RISC channels are highlighted by pink color.

In principle, **T-CNDF-T-*t*Cz** have three quasi equivalent donor and acceptor, which could promote the RISC process in resonance by degenerating singlet and triplet levels.[10] Thus we then performed first principles TD-DFT investigations, natural bond orbital (NBO) analysis, and spin–orbit coupling (SOC) calculations.[29, 30] Ground state electronic structure of **T-CNDF-T-*t*Cz** shows that HOMO-2 ($E_{H2} = -6.305$, **Figure S1c**), HOMO-1 ($E_{H1} = -6.305$, **Figure S1d**), and HOMO ($E_H = -6.219$, **Figure S1e**), as well as the LUMO ($E_L = -2.541$, **Figure S1f**) and LUMO+1 ($E_{L1} = -2.541$, **Figure S1g**) are nearly degenerated. Accordingly, from the TD-DFT calculated excited states of **T-CNDF-T-*t*Cz**, singlet (S_1–S_6) and triplet

excited states (T_2−T_6) have similar energy levels (**Table S3**), which are close to T_1 with small ΔE_{SnTn}s (n ≤ 6) to support an efficient multi-channel RISC process. In contrast, **S-CNDF-S-*t*Cz** and **S-CNDF-D-*t*Cz** with fewer donor/acceptor units, the S_n and T_n states are considerably different. As illustrated in **Figure 2** and **Table S4**, the numbers of the valid RISC channels with both small ΔE_{ST} (≤ 0.37 eV) and high SOC values (≥ 0.3 cm^{-1})[29, 30] are determined to be 0, 5, and 8, respectively, for **S-CNDF-S-*t*Cz**, **S-CNDF-D-*t*Cz**, and **T-CNDF-T-*t*Cz**. All these results suggest that the RISC process from T_n to S_n in **T-CNDF-T-*t*Cz** is more effective than in the reference compounds. Consequently, the multi-(donor/acceptor) molecule possesses much efficient triplet-harnessing abilities, and thereby may enhance their light-emitting performances under the optical or electrical excitations.

All compounds were synthesized by Pd-catalyzed Suzuki crossing-coupling reactions of different halogen (Br or I)-substituted ***t*Cz** units with the corresponding **CNDF**-borate in moderate yield (**Scheme S1**). Their molecular structures were well characterized by ^{1}H NMR, ^{13}C NMR, high-resolution mass spectrometry (HRMS), and single crystal structure analysis. As shown in **Figure 3**, the crystal structures confirm that the centroid-centroid distances between donor ***t*Cz** and acceptor **CNDF** among these compounds are less than 3.3 Å, which may allow the efficient TSCT to achieve delayed fluorescence. In addition, all the molecular structures are highly twisted, the dihedral angles between the ***t*Cz** units and the adjacent phenyl bridges are 55.2° for **S-CNDF-S-*t*Cz**, 61.7° for **S-CNDF-D-*t*Cz**, and 74.9° for **T-CNDF-T-*t*Cz**, illustrating the coexistence of TSCT and TBCT effects within these compounds. Notably, the packing diagram of **T-CNDF-T-*t*Cz** demonstrates that the multi-(donor/acceptor) molecule exhibits negligible intermolecular interactions (**Figure S2**), which makes it a suitable emitter for the non-doped OLEDs. All these results are in close agreement with the conclusions obtained from the TD-DFT simulation. Therefore, we

anticipate that the multi-(donor/acceptor) molecule combining the TSCT and TBCT effects could be a good candidate for high-performance TADF-OLEDs.

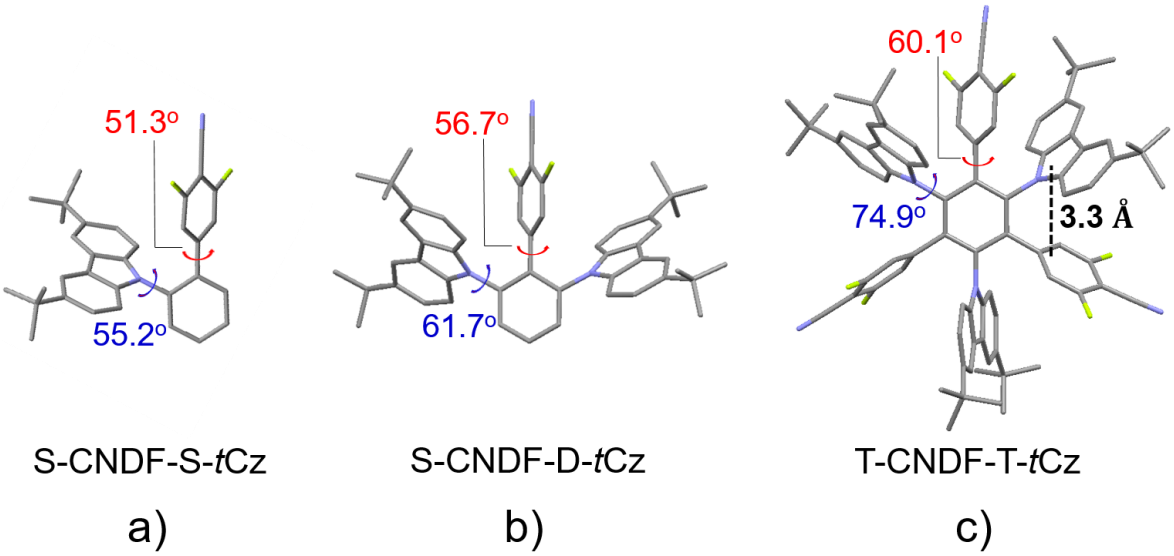

Figure 3. The single crystal structures of **S-CNDF-S-*t*Cz** (a), **S-CNDF-D-*t*Cz** (b), and **T-CNDF-T-*t*Cz** (c). The values of dihedral angels and distances are the averaged ones obtained from the corresponding crystal structures. For all crystal structures, the disordered solvent molecules and hydrogen atoms are omitted for the sake of clarity. Carbon, gray; nitrogen, blue; fluorine, yellow green.

The UV-Vis absorption in chloroform (1×10^{-4} M) and photoluminescence (PL) spectra in the neat films of **S-CNDF-S-*t*Cz**, **S-CNDF-D-*t*Cz**, and **T-CNDF-T-*t*Cz** are shown in **Figure 4**, and data are summarized in **Table 1**. All emitters demonstrate an absorption band at about 330 nm attributed to the local transition of **ph-*t*Cz** or **ph-CNDF**, and a CT band in the range of 360-420 nm originating from the CT-transition from the donor to the acceptor. The emission peak of **T-CNDF-T-*t*Cz** reveals a bathochromic shift of approximately 30 nm compared with **S-CNDF-S-*t*Cz** or **S-CNDF-D-*t*Cz** due to the more donor-acceptor units. The CT characteristics of these compounds are also inferred by the absorption and emission spectra in solvents with different polarities (**Figure S3**). Taking **T-CNDF-T-*t*Cz** as an example, with the increasing solvent polarity, the emission maximum displays a distinct

positive solvatochromism (*e.g.*, λ_{PLmax} = 450 nm in toluene, 472 nm in chloroform, and 550 nm in acetone). According to the onsets of fluorescence and phosphorescence spectra of these emitters in their neat films, the ΔE_{ST} of **S-CNDF-S-*t*Cz**, **S-CNDF-D-*t*Cz**, and **T-CNDF-T-*t*Cz** are estimated to be 0.24, 0.21, and 0.03 eV, respectively, confirming the multi-(donor/acceptor) molecule could degenerate frontier orbitals and thus result in a small energy gap, which will effectively improve the RISC process by means of up-conversion from T_n to S_n.

Subsequently, we conducted the measurement for the transient PL decay curves of these compounds at room temperature. As shown in **Figures S4, S5, S6** and **Table S1**, in degassed chloroform, **T-CNDF-T-*t*Cz** displays a distinctive delayed emission with a lifetime (τ_d) of 7.5 μs, together with a prompt emission with lifetime (τ_p) of 13 ns. The delayed component percentage is 92% and the prompt component is 8%. However, when exposing this solution to air, the delayed component is inconspicuous, indicating that the delayed emission of **T-CNDF-T-*t*Cz** is originated from the triplets which are effectively quenched by oxygen (**Figure S5e**).[16] Similar experimental phenomena could also be observed in its non-doped film (**Figure 4f**). The temperature dependent time-resolved measurements for **S-CNDF-S-*t*Cz**, **S-CNDF-D-*t*Cz** and **T-CNDF-T-*t*Cz** were performed as shown in **Figure 5**. All the curves exhibit two clear components, prompt fluorescence (PF) in nanosecond scale and DF in microsecond scale in these three compounds. The positive temperature dependence of the decays in DF region and linear proportionality of DF intensity *vs.* laser pumping power reveal the monomolecular process, further confirming their TADF mechanism.

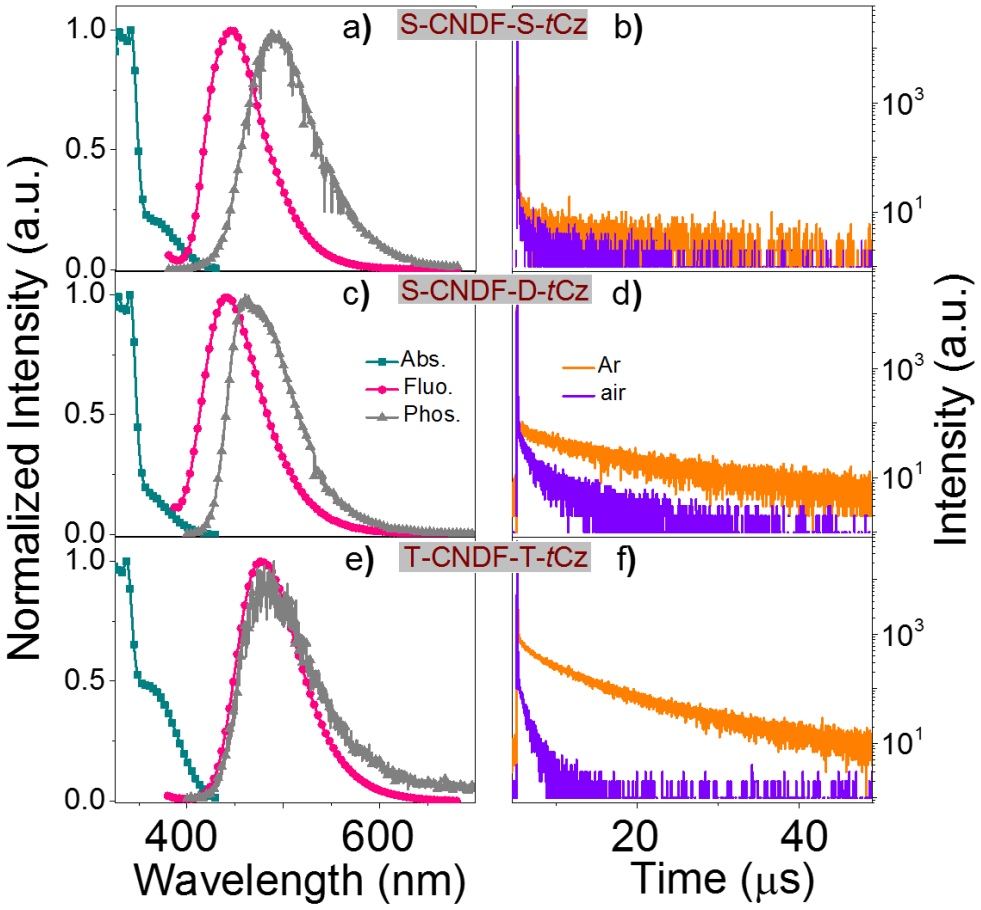

Figure 4. Normalized absorption spectra (green-blue trace) measured at room temperature in chloroform (1×10^{-4} M), normalized fluorescence spectra (red trace) at room temperature and phosphorescence spectra (gray trace) at 77 K in neat films of **S-CNDF-S-*t*Cz** (a), **S-CNDF-D-*t*Cz** (c), and **T-CNDF-T-*t*Cz** (e). Fluorescence decay curves of **S-CNDF-S-*t*Cz** (b), **S-CNDF-D-*t*Cz** (d), and **T-CNDF-T-*t*Cz** (f) in neat film states at 298 K (monitored at 460 nm) under aerated (purple color) and degassed (orange color) condition.

The TD-DFT calculations forecast that both TBCT and TSCT are involved in the TADF emission in these compounds. To clarify the suggested mechanism, a *para*-substituted molecule ***p*-S-CNDF-S-*t*Cz** was investigated in comparison to its isomer **S- CNDF-S-*t*Cz** with the D unit substituted at the *ortho* position of the A unit. In ***p*-S-CNDF-S-*t*Cz**, the TSCT seems not to be effective as the *para*-substitution increases the spatial distance between the D and A units. As shown in **Figure S7**, a strong CT character is clearly observed, which is safely attributed to the TBCT effect. Thus it is proposed that the TBCT is active and dominant in the *para*-substituted molecule ***p*-S-CNDF-S-*t*Cz**. As expected, no TADF is observed due to

the large energy gap (0.44 eV, **Figure S8**). This indicates that only TBCT exists in ***p*-S-CNDF-S-*t*Cz** to give the CT character. The results give clear evidence that the contribution of TADF in **S-CNDF-S-*t*Cz** originates from both TBCT and TSCT effects. With the increasing numbers of D/A units in **S-CNDF-D-*t*Cz** and **T-CNDF-T-*t*Cz**, a large density of triplet pathways given by more D/A channels *via* TBCT and TSCT and there is no doubt that TSCT accelerates the RISC process due to the further reduced ΔE_{ST} in **T-CNDF-T-*t*Cz**. Therefore, more efficient TADF is observed in the multi-D/A system. All these results are in good agreement with the TD-DFT calculated data.

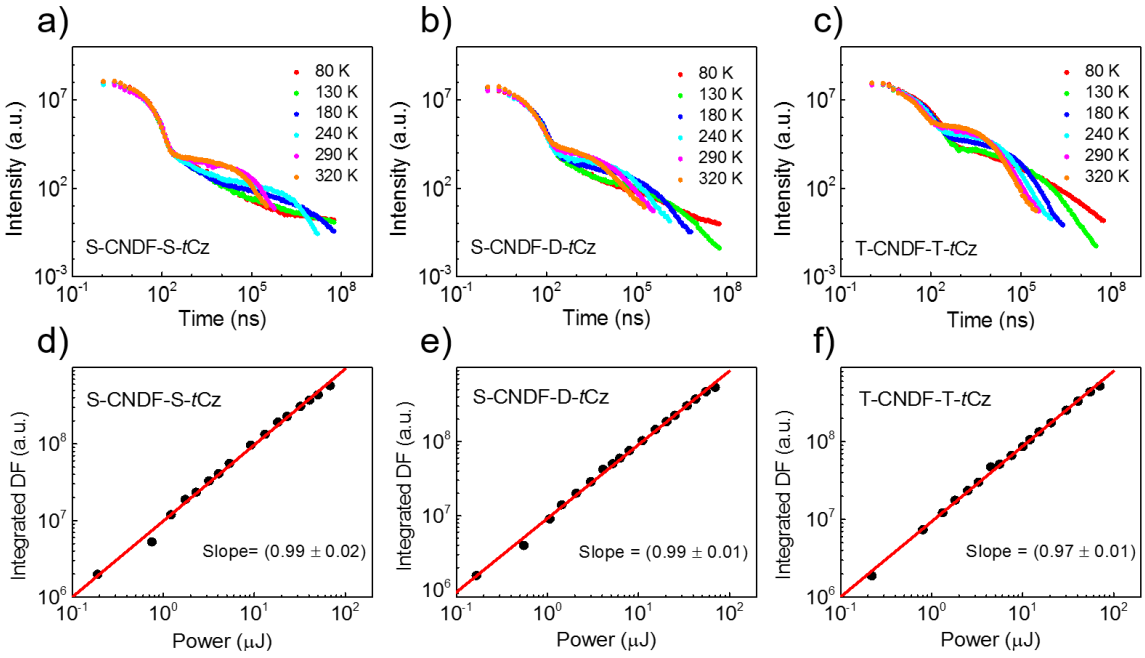

Figure 5. Temperature dependent time-resolved decays of **S-CNDF-S-*t*Cz** (a), **S-CNDF-D-*t*Cz** (b) and **T-CNDF-T-*t*Cz** (c) in neat films from 320 K to 80 K. Power dependent measurements of **S-CNDF-S-*t*Cz** (d), **S-CNDF-D-*t*Cz** (e) and **T-CNDF-T-*t*Cz** (f) with delay/integration time of 0.6/200 μs, 0.6/200 μs, and 0.5/100 μs, respectively, collected at room temperature.

Besides, the anti-stacking crystal pattern of **T-CNDF-T-*t*Cz** may allow it to avoid fluorescence quenching in the pristine state.[27] Then, we evaluated the PLQYs of these three compounds in the neat films. As listed in **Table 1**, the absolute PLQYs in air-saturated thin

film are 31% for **S-CNDF-S-*t*Cz**, 6% for **S-CNDF-D-*t*Cz**, and 19% for **T-CNDF-T-*t*Cz**. In contrast, the degassed samples give the corresponding values of 42%, 19% and 76%, sequentially. Obviously, in the presence of oxygen, the PLQY of **T-CNDF-T-*t*Cz** has been significantly reduced, which may be ascribed to the larger density of T_ns which are easily quenched by oxygen. The rate constants of RISC (k_{RISC}) were estimated using a previously reported method[31] to be $(0.12 \pm 0.05) \times 10^5$ s^{-1}, $(2.27 \pm 0.30) \times 10^5$ s^{-1} and $(5.07 \pm 0.65) \times 10^5$ s^{-1}, respectively, for **S-CNDF-S-*t*Cz**, **S-CNDF-D-*t*Cz**, and **T-CNDF-T-*t*Cz** (**Figure S9**). In comparison with the reference molecules, the k_{RISC} value of multi-(donor/acceptor) molecule was distinctly enhanced, evidencing a more efficient RISC process in **T-CNDF-T-*t*Cz** due to the increased density of triplet pathways. The promising luminescent behavior of **T-CNDF-T-*t*Cz** both in solution and film state clearly demonstrated the success of our unique design strategy for efficient TADF features.

Table 1. Photophysical parameters of **S-CNDF-S-*t*Cz**, **S-CNDF-D-*t*Cz**, and **T-CNDF-T-*t*Cz**.

Compound	λ_{abs} (nm)[a]	λ_{em} (nm)[b]	E_S/E_T (eV)[c]	ΔE_{ST} (eV)[d]	τ_p (ns)[e]	τ_d (μs)[f]	Φ_{PL}/Φ_F (%)[g]
S-CNDF-S-*t*Cz	340/367	476/445	3.08/2.84	0.24	17.0	1.83/54.3	42/31
S-CNDF-D-*t*Cz	340/366	466/441	3.11/2.90	0.21	14.1	2.20/13.4	19/6
T-CNDF-T-*t*Cz	337/362	472/477	2.88/2.85	0.03	21.3	1.65/7.79	76/19

[a]Measured in chloroform (1×10^{-4} M) at room temperature. [b]Measured in chloroform (1×10^{-4} M) (former) and neat film (latter) at room temperature, respectively. [c]E_S and E_T obtained from the onsets of fluorescence and phosphorescence spectra of these emitters in the neat films. [d]ΔE_{ST} calculated from $E_S - E_T$. [e]Prompt and [f]delayed fluorescence lifetimes in the neat films at room temperature, fitted from the time-resolved decays. [g]Φ_{PL} and Φ_F represent the PLQYs of the deoxygenated and air-saturated neat films, respectively (Excitation wavelength is 360 nm). [h]Rate constant of RISC process.

Therefore, we fabricated the solution-processed devices using the multi-(donor/acceptor) molecule, **T-CNDF-T-*t*Cz**, as a non-doped emitting material. The structure of device A is ITO/PEDOT:PSS (40 nm)/**T-CNDF-T-*t*Cz** (45 nm)/DPEPO (10 nm)/TmPyPB (50 nm)/Liq (1 nm)/Al (100 nm) (**Figure 6a**), where

poly(3,4-ethylenedioxythiophene):poly(styrenesulfonic acid) (PEDOT:PSS) and 8-hydroxyquinolinolato-lithium (Liq) served as the hole- and electron-injection layer, respectively; 1,3,5-tri(m-pyrid-3-yl-phenyl)benzene (TmPyPB) acted as the electron-transporting layer; and bis(2-(diphenylphosphino)phenyl)ether oxide (DPEPO) was used as the hole-blocking layer. We also fabricated two reference devices employing **S-CNDF-S-*t*Cz** (device B) and **S-CNDF-D-*t*Cz** (device C) in the same device configurations for comparison.

The voltage–current density, voltage–brightness characteristics, EL spectrum and the efficiency as a function of the current density of these devices are illustrated in **Figures 6**, **S12** and the data are summarized in **Table 2**. Device A based on **T-CNDF-T-*t*Cz** shows a sky-blue emission peaking at 484 nm, and achieved B_{max} of 5210 cd m^{-2}, a maximum current efficiency (CE_{max}) of 46.4 cd A^{-1}, a maximum power efficiency (PE_{max}) of 20.8 lm W^{-1}, and an EQE_{max} of 21.0%. To the best of our knowledge, the EL performances of the multi-(donor/acceptor)-based device are evidently superior to those reported previously, and achieved the record efficiency among sky-blue OLEDs fabricated by solution process. Comparatively, the EL performances of the reference devices B and C are much inferior, with the B_{max}, CE_{max}, PE_{max}, and EQE_{max} of 474 cd m^{-2}, 3.6 cd A^{-1}, 1.4 lm W^{-1}, and 2.6% for **S-CNDF-S-*t*Cz**, and 659 cd m^{-2}, 5.0 cd A^{-1}, 2.2 lm W^{-1}, and 3.7% for **S-CNDF-D-*t*Cz**, respectively. Particularly, the *EQEs* drastically drop from 21% (**T-CNDF-T-*t*Cz**, three-D/A) to 2.6% (**S-CNDF-S-*t*Cz**, single D/A). Furthermore, the η_r (exciton utilization efficiency) of these devices was estimated according to equation ($\eta_{ext} = \gamma \cdot \eta_r \cdot \Phi_{PL} \cdot \eta_{out}$), where η_{out} represents the light out-coupling efficiency (for glass substrates, $\eta_{out} \approx 25-30\%$), γ is the charge balance factor (for a properly device, $\gamma = 1$). Considering the Φ_{PL} of 76% for **T-CNDF-T-*t*Cz**, barely in its own film, the estimated η_r of this multi-(donor/acceptor)-based device was approaching 100%, indicating that almost all the electrically generated excitons are radiative. The fact that

the higher efficiency in device A may be ascribed to the much higher PLQY and faster RISC process induced by the multi-(donor/acceptor) nature together with the simultaneous TSCT and TBCT effects in **T-CNDF-T-*t*Cz** compared with the reference molecules, which clearly evidence the effectiveness and flexibility of our design strategy.

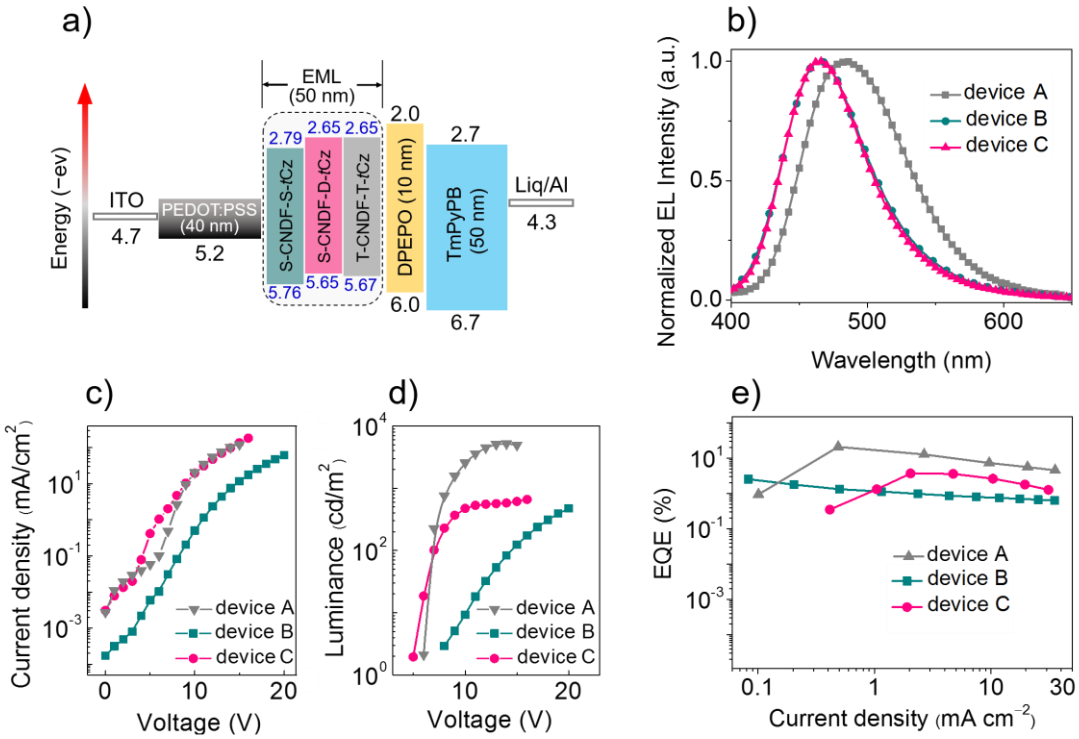

Figure 6. (a) Solution-processed device configurations of **S-CNDF-S-*t*Cz, S-CNDF-D-*t*Cz, and T-CNDF-T-*t*Cz** employed device A, B, and C; EL spectrum (b), voltage–current density (*V*–*J*) characteristics (c), voltage–luminance (*V*–*L*) characteristics (d), and External quantum efficiency (e) of the devices A, B, and C.

Table 2. Summary of the EL Data of the devices A, B, and C employing **T-CNDF-T-*t*Cz**, **S-CNDF-S-*t*Cz**, and **S-CNDF-D-*t*Cz**, respectively.

Device	Emitting layers	V_{on} (V)[a]	B_{max} (cd m^{-2})[b]	CE_{max} (cd A^{-1})[c]	PE_{max} (lm W^{-1})[d]	EQE_{max} (%)[e]	λ_{em} (nm)[f]	CIE (x,y)[g]
A	**T-CNDF-T-*t*Cz**	6.3	5210	46.4	20.8	21.0	484	(0.19, 0.35)
B	**S-CNDF-S-*t*Cz**	10.1	474	3.6	1.4	2.6	466	(0.16, 0.18)
C	**S-CNDF-D-*t*Cz**	5.7	659	5.0	2.2	3.7	466	(0.16, 0.17)

[a]The operation voltage recorded at a brightness of 10 cd m^{-2}. [b]The maximum brightness (B_{max}). [c]The maximum current efficiency (CE_{max}). [d]The maximum power efficiency (PE_{max}). [e]The maximum external quantum efficiency (EQE_{max}). [f]The EL peak wavelength and [g]Commission International de I'Eclairage coordinates.

In summary, we proposed a novel and efficient molecular design strategy for the construction of high-performance TADF materials by introducing multiple alternating donor and acceptor units onto the π bridge (like benzene ring). The co-existence of through-space and through-bond charge transfer ensures the molecule, targeting for blue emission, to possess a very small energy gap and large transition dipole moment concurrently. Additionally, the highly twisted structure of the multi-(donor/acceptor) systems can not only efficiently inhibit aggressive quenching to obtain a high PLQY, but also potentially degenerate molecular orbitals, leading to the opening of more RISC channels. Eventually, the three-(donor/acceptor) TADF molecule, **T-CNDF-T-*t*Cz**, was ensured with a small singlet-triplet gap, high quantum yield, and fast RISC process. Hence, it shows much superior EL efficiencies than the reference molecules with fewer donor/acceptor units, **S-CNDF-S-*t*Cz** and **S-CNDF-D-*t*Cz**, *e.g.*, 21% *vs.* 2.6 and 3.7%, respectively, in terms of EQE_{max}. It is worth mentioning that the *EQE* of the device employing **T-CNDF-T-*t*Cz** champions blue solution-processed TADF OLEDs with the neat emitters. Evidently, this facile constructive strategy for TADF molecules would greatly extend the design rationales, which will light up the enthusiasm of scientists to develop more promising TADF materials for flat panel displays and lighting applications.

Supporting Information

Supporting Information is available online from the Wiley Online Library or from the author.

Acknowledgements

Xujun Zheng and Rongjuan Huang contributed equally to this work. The authors would like to thank the financial support from the National Natural Science Foundation of China (Project Nos. 91833304, 61575146, 51873159, 21721005, and 91433201), National Key R&D Program of China (Project No. 2016YFB0401002), the National Basic Research Program of China (973 Program 2015CB655002), Shenzhen Peacock Plan (KQTD20170330110107046), the Key Technological Innovation Program of Hubei Province (2018AAA013), and the Natural Science Foundation of Hubei Province (2017CFB687). FMBD and GX thank the Royal Society, UK for the funding, IEC\NSFC\170130–International Exchanges 2017 Cost Share (China).

Received: ((will be filled in by the editorial staff))

Revised: ((will be filled in by the editorial staff))

Published online: ((will be filled in by the editorial staff))

[1] M. Segal, M. A. Baldo, R. J. Holmes, S. R. Forrest, Z. G. Soos, *Phys. Rev. B* **2003**, *68*, 075211.

[2] H. Uoyama, K. Goushi, K. Shizu, H. Nomura, C. Adachi, *Nature* **2012**, *492*, 234.

[3] Q. Zhang, J. Li, K. Shizu, S. Huang, S. Hirata, H. Miyazaki, C. Adachi, *J. Am. Chem. Soc.* **2012**, *134*, 14706.

[4] Q. Zhang, H. Kuwabara, W. J. Potscavage, S. Huang, Y. Hatae, T. Shibata, C. Adachi, *J. Am. Chem. Soc.* **2014**, *136*, 18070.

[5] H. Kaji, H. Suzuki, T. Fukushima, K. Shizu, K. Suzuki, S. Kubo, T. Komino, H. Oiwa, F. Suzuki, A. Wakamiya, Y. Murata, C. Adachi, *Nat. Commun.* **2015**, *6*, 8476.

[6] T. Hosokai, H. Matsuzaki, H. Nakanotani, K. Tokumaru, T. Tsutsui, A. Furube, K. Nasu, H. Nomura, M. Yahiro, C. Adachi, *Sci. Adv.* **2017**, *3*, e1603282.

[7] M. A. Baldo, D. F. O'Brien, Y. You, A. Shoustikov, S. Sibley, M. E. Thompson, S. R. Forrest, *Nature* **1998**, *395*, 151.

[8] K. Tuong Ly, R.-W. Chen-Cheng, H.-W. Lin, Y.-J. Shiau, S.-H. Liu, P.-T. Chou, C.-S. Tsao, Y.-C. Huang, Y. Chi, *Nat. Photonics* **2016**, *11*, 63.

[9] M. Sarma, W.-L. Tsai, W.-K. Lee, Y. Chi, C.-C. Wu, S.-H. Liu, P.-T. Chou, K.-T. Wong, *Chem* **2017**, *3*, 461.

[10] P. L. dos Santos, J. S. Ward, D. G. Congrave, A. S. Batsanov, J. Eng, J. E. Stacey, T. J. Penfold, A. P. Monkman, M. R. Bryce, *Adv. Sci*. **2018**, *5*, 1700989.

[11] R. Furue, T. Nishimoto, I. S. Park, J. Lee, T. Yasuda, *Angew. Chem., Int. Ed*. **2016**, *55*, 7171.

[12] D. R. Lee, M. Kim, S. K. Jeon, S.-H. Hwang, C. W. Lee, J. Y. Lee, *Adv. Mater.* **2015**, *27*, 5861.

[13] H. Liu, J. Zeng, J. Guo, H. Nie, Z. Zhao, B. Z. Tang, *Angew. Chem., Int. Ed*. **2018**, *57*, 9290.

[14] Y.-J. Shiu, Y.-C. Cheng, W.-L. Tsai, C.-C. Wu, C.-T. Chao, C.-W. Lu, Y. Chi, Y.-T. Chen, S.-H. Liu, P.-T. Chou, *Angew. Chem., Int. Ed*. **2016**, *55*, 3017.

[15] W.-L. Tsai, M.-H. Huang, W.-K. Lee, Y.-J. Hsu, K.-C. Pan, Y.-H. Huang, H.-C. Ting, M. Sarma, Y.-Y. Ho, H.-C. Hu, C.-C. Chen, M.-T. Lee, K.-T. Wong, C.-C. Wu, *Chem. Commun.* **2015**, *51*, 13662.

[16] K. Kawasumi, T. Wu, T. Zhu, H. S. Chae, T. Van Voorhis, M. A. Baldo, T. M. Swager, *J. Am. Chem. Soc.* **2015**, *137*, 11908.

[17] X. Wang, S. Wang, J. Lv, S. Shao, L. Wang, X. Jing, F. Wang, *Chem. Sci*. **2019**, *10*, 2915.

[18] J. W. Sun, J. H. Lee, C. K. Moon, K. H. Kim, H. Shin, J. J. Kim, *Adv. Mater.* **2014**, *26*, 5684.

[19] P. Zhang, J. Zeng, J. Guo, S. Zhen, B. Xiao, Z. Wang, Z. Zhao, B. Z. Tang, *Front. Chem*. **2019**, *7*, 199.

[20] T. Huang, W. Jiang, L. Duan, *J. Mater. Chem. C* **2018**, *6*, 5577.

[21] Y. Zou, S. Gong, G. Xie, C. Yang, *Adv. Opt. Mater.* **2018**, *6*, 1800568.

[22] A. C. Arias, J. D. MacKenzie, I. McCulloch, J. Rivnay, A. Salleo, *Chem. Rev*. **2010**, *110*, 3.

[23] K. S. Yook, S. E. Jang, S. O. Jeon, J. Y. Lee, *Adv. Mater.* **2010**, *22*, 4479.

[24] Y. Wada, S. Kubo, H. Kaji, *Adv. Mater.* **2018**, *30*, 1705641.

[25] X. L. Chen, J. H. Jia, R. Yu, J. Z. Liao, M. X. Yang, C. Z. Lu, *Angew. Chem., Int. Ed.* **2017**, *56*, 15006.

[26] J.-T. Ye, L. Wang, H.-Q. Wang, X.-M. Pan, H.-M. Xie, Y.-Q. Qiu, *J. Phys. Chem. C* **2018**, *122*, 18850.

[27] J. Mei, N. L. C. Leung, R. T. K. Kwok, J. W. Y. Lam, B. Z. Tang, *Chem. Rev*. **2015**, *115*, 11718.

[28] Y. Hong, J. W. Y. Lam, B. Z. Tang, *Chem. Soc. Rev*. **2011**, *40*, 5361.

[29] R. Chen, Y. Tang, Y. Wan, T. Chen, C. Zheng, Y. Qi, Y. Cheng, W. Huang, *Sci. Rep.* **2017**, *7*, 6225.

[30] Y. Tao, R. Chen, H. Li, J. Yuan, Y. Wan, H. Jiang, C. Chen, Y. Si, C. Zheng, B. Yang, G. Xing, W. Huang, *Adv. Mater.* **2018**, *30*, 1803856.

[31] K.-C. Pan, S.-W. Li, Y.-Y. Ho, Y.-J. Shiu, W.-L. Tsai, M. Jiao, W.-K. Lee, C.-C. Wu, C.-L. Chung, T. Chatterjee, Y.-S. Li, K.-T. Wong, H.-C. Hu, C.-C. Chen, M.-T. Lee, *Adv. Funct. Mater.* **2016**, *26*, 7560.

A novel multi-(donor/acceptor) TADF molecule with through-space/-bond charge transfer was developed. Compared to the reference molecules with fewer donor/acceptor units, it exhibits a small singlet-triplet gap, high quantum yield, and fast RISC process. Hence, the non-doped solution-processed sky-blue OLED displays high performance with an external quantum efficiency (EQE_{max}) up to 21.0%, which represents the record-breaking efficiency among the solution processes-based non-doped sky-blue OLEDs.